Atmos. Chem. Phys., 16, 4439–4449, 2016
www.atmos-chem-phys.net/16/4439/2016/
doi:10.5194/acp-16-4439-2016

Atmospheric Chemistry and Physics Open Access EGU

Kinetic isotope effects of $^{12}CH_3D + OH$ and $^{13}CH_3D + OH$ from 278 to 313 K

L. M. T. Joelsson[1,3], J. A. Schmidt[1], E. J. K. Nilsson[2], T. Blunier[3], D. W. T. Griffith[4], S. Ono[5], and M. S. Johnson[1]

[1]Department of Chemistry, University of Copenhagen, Copenhagen, Denmark
[2]Division of Combustion Physics, Department of Physics, Lund University, Lund, Sweden
[3]Centre for Ice and Climate (CIC), Niels Bohr Institute, University of Copenhagen, Copenhagen, Denmark
[4]University of Wollongong, Department of Chemistry, Wollongong, Australia
[5]Department of Earth, Atmospheric and Planetary Sciences, Massachusetts Institute of Technology, Cambridge, MA, USA

Correspondence to: M. S. Johnson (msj@chem.ku.dk)

Received: 16 September 2015 – Published in Atmos. Chem. Phys. Discuss.: 15 October 2015
Revised: 2 March 2016 – Accepted: 16 March 2016 – Published: 11 April 2016

Abstract. Methane is the second most important long-lived greenhouse gas and plays a central role in the chemistry of the Earth's atmosphere. Nonetheless there are significant uncertainties in its source budget. Analysis of the isotopic composition of atmospheric methane, including the doubly substituted species $^{13}CH_3D$, offers new insight into the methane budget as the sources and sinks have distinct isotopic signatures. The most important sink of atmospheric methane is oxidation by OH in the troposphere, which accounts for around 84 % of all methane removal. Here we present experimentally derived methane + OH kinetic isotope effects and their temperature dependence over the range of 278 to 313 K for CH_3D and $^{13}CH_3D$; the latter is reported here for the first time. We find $k_{CH_4}/k_{CH_3D} = 1.31 \pm 0.01$ and $k_{CH_4}/k_{^{13}CH_3D} = 1.34 \pm 0.03$ at room temperature, implying that the methane + OH kinetic isotope effect is multiplicative such that $(k_{CH_4}/k_{^{13}CH_4})(k_{CH_4}/k_{CH_3D}) = k_{CH_4}/k_{^{13}CH_3D}$, within the experimental uncertainty, given the literature value of $k_{CH_4}/k_{^{13}CH_4} = 1.0039 \pm 0.0002$. In addition, the kinetic isotope effects were characterized using transition state theory with tunneling corrections. Good agreement between the experimental, quantum chemical, and available literature values was obtained. Based on the results we conclude that the OH reaction (the main sink of methane) at steady state can produce an atmospheric clumped isotope signal ($\Delta(^{13}CH_3D) = \ln([CH_4][^{13}CH_3D]/[^{13}CH_4][CH_3D])$) of 0.02 ± 0.02. This implies that the bulk tropospheric $\Delta(^{13}CH_3D)$ reflects the source signal with relatively small adjustment due to the sink signal (i.e., mainly OH oxidation).

1 Introduction

Atmospheric methane is the subject of increasing interest from both the climate research community and the public due its impacts on climate change, as reported by the IPCC (2013). The direct radiative forcing of methane is $0.64\,W\,m^{-2}$. Including feedback mechanisms and secondary effects (e.g., increased O_3 production, stratospheric water vapor, and production of CO_2), methane's radiative forcing becomes $0.97\,W\,m^{-2}$, two-thirds of the forcing by CO_2 over the same time period (IPCC, 2013, Fig. 8.15).

Atmospheric methane has both natural and anthropogenic sources and the two categories contribute about equally (Ciais et al., 2013, and references therein). Wetlands are the dominant natural source, and agriculture and waste are the largest anthropogenic sources. Fossil fuels make smaller contributions. The majority (84 %) of atmospheric methane is removed by oxidation by OH in the troposphere:

$$CH_4 + OH \rightarrow CH_3 + H_2O, \quad \text{(R1)}$$

while oxidation in the troposphere by Cl contributes about 4 % of the total:

$$CH_4 + Cl \rightarrow CH_3 + HCl. \quad \text{(R2)}$$

About 8 % of methane is removed in the stratosphere by radical oxidation, such as Reactions (R1), (R2) and (R3):

$$CH_4 + O(^1D) \rightarrow CH_3 + OH. \quad \text{(R3)}$$

The rest (4 %) is removed by soil (Kirschke et al., 2013).

Carbon and hydrogen isotopic analyses are widely used to distinguish microbial and thermal sources of atmospheric methane (e.g., Lowe et al., 1997; Ferretti et al., 2005; Tyler et al., 2007; Lassey et al., 2007). However, Reactions (R1), (R2), and (R3) produce relatively large D/H isotope effects (Saueressig et al., 1995, 1996, 2001; Crowley et al., 1999; Feilberg et al., 2005). Thus, the construction of an accurate top-down methane budget by isotopic analysis must take the isotopic signatures of both sources and sinks into account (Quay et al., 1999; Bergamaschi et al., 2000; Allan et al., 2001a, b). An isotope budget based on methane source (and sink) fractionations is an underdetermined systems (e.g., Pohlman et al., 2009). Recent advances in mass spectrometry (Eiler et al., 2013; Stolper et al., 2014) and laser infrared spectroscopy (Ono et al., 2014; Wang et al., 2015) facilitate measurement of rare doubly substituted isotopologues. The abundance of these "clumped" isotopologues (clumped refers to the rare isotopes being clumped together) generally follows a stochastic distribution (i.e., $[^{12}CH_4][^{13}CH_3D] = [^{13}CH_4][^{12}CH_3D]$). However, small deviations from stochastic distribution can be induced by thermodynamic (Ma et al., 2008; Stolper et al., 2014; Liu and Liu, 2016), kinetic (Joelsson et al., 2014; Wang et al., 2015), and photolytic processes (Schmidt et al., 2013; Schmidt and Johnson, 2015). Analysis of the clumped isotope anomaly in methane will yield unique constraints for the methane budget. Optical methods, as will be shown in this paper, provide high throughput and accuracy for overcoming the problems of analysis of clumped CH_4. The difference and advantage of this approach is the additional information not available in single-isotope analysis, especially regarding the mechanism of formation, independent of the enrichment of D and ^{13}C in the starting material.

The kinetic isotope effect, ${}^{j\mathrm{E}}\alpha$, is a characteristic property of each process:

$${}^{j\mathrm{E}}\alpha \equiv \frac{k({}^{i}\mathrm{E} + \mathrm{OH})}{k({}^{j}\mathrm{E} + \mathrm{OH})}, \quad (1)$$

where ${}^{i}\mathrm{E}$ is the most abundant (here, the lighter) isotopologue, ${}^{j}\mathrm{E}$ the rare (heavy) isotopologue, and $k(\mathrm{E} + \mathrm{OH})$ the reaction rate coefficient for the reaction $\mathrm{E} + \mathrm{OH}$. As a measure of how much of a fractionation of $^{13}CH_3D$ kinetic reactions produce, the apparent clumpiness, γ, is used. It is a measure of the effect of the clumped substitution on the reaction rate, as opposed to the combined effect of two single substitutions. It is defined as (Wang et al., 2015)

$$\gamma \equiv \frac{{}^{13\mathrm{C,D}}\alpha}{{}^{13\mathrm{C}}\alpha \times {}^{\mathrm{D}}\alpha}. \quad (2)$$

A related measure is the $\Delta(^{13}CH_3D)$ value that quantifies the extent to which rare isotopes clump together to form a multiply substituted species, as opposed to a stochastic distribution (Ono et al., 2014):

$$\Delta(^{13}CH_3D) \equiv \ln\left(\frac{[^{13}CH_3D][^{12}CH_4]}{[^{12}CH_3D][^{13}CH_4]}\right), \quad (3)$$

where $[^{13}CH_3D]$, $[^{12}CH_4]$, $[^{12}CH_3D]$, and $[^{13}CH_4]$ represent the concentrations of the different isotopologues.

The kinetic isotope effects for the singly substituted species CH_3D and $^{13}CH_4$ have been studied previously both experimentally and theoretically; see Tables 3 and 4, respectively. The kinetic isotope effect ${}^{13\mathrm{C,D}}\alpha$ for the reaction with OH is not described in the existing literature. The related kinetic isotope effect for the $CH_4 + Cl$ reaction was measured at room temperature with the present setup by Joelsson et al. (2014) and found to be 1.60 ± 0.04. The kinetic isotope effects in the doubly substituted methane isotopologue CH_2D_2 for the reaction $CH_4 + Cl$ has been studied previously by Feilberg et al. (2005).

In the present study the kinetic isotope effects ${}^{\mathrm{D}}\alpha$ and ${}^{13\mathrm{C,D}}\alpha$ are determined using the relative rate method. Species concentrations in the reaction cell are determined using Fourier transform infrared (FTIR) spectroscopy. Further, ${}^{\mathrm{D}}\alpha$, ${}^{13\mathrm{C}}\alpha$, and ${}^{13\mathrm{C,D}}\alpha$ are calculated using quantum chemistry and transition state theory.

2 Experimental procedures

Sixteen experiments were conducted, numbered from 1 through 16 (see Table 1): eight (Experiments 1–8) for $^{12}CH_3D$ and eight (Experiments 9–16) for $^{13}CH_3D$. The experiments were conducted at four different temperatures ($T = 278$, 288, 298, 313 K = 5, 15, 25, 40 °C); two experiments were conducted for each temperature.

2.1 Relative rate method

The experiments were carried out using the relative rate method on a semi-static gas mixture. The decaying concentrations of reactants were measured as a function of the extent of reaction. Considering two bimolecular reactions with second-order rate coefficients k_A and k_B,

$$A + OH \xrightarrow{k_A} \text{products}, \quad \text{(R4)}$$

$$B + OH \xrightarrow{k_B} \text{products}, \quad \text{(R5)}$$

and assuming there were no other loss processes, the following relation holds:

$$\ln\left(\frac{[A]_0}{[A]_t}\right) = \frac{k_A}{k_B} \ln\left(\frac{[B]_0}{[B]_t}\right). \quad (4)$$

Here $[A]_0$, $[A]_t$, $[B]_0$, and $[B]_t$ represent the concentrations of compounds A and B at times 0 and t, respectively. The

Table 1. Experimental setup. The experiment numbers are listed in column Exp., the detector is listed in column Detect., the heavy CH_4 isotopologue included in the experiments is listed in column [$^xCH_3D$], the mean measured temperatures in the photoreactor are listed in column T, the H_2O vapor concentrations at the start of the experiments ($t = 0$) as obtained from spectral fitting are listed in column $[H_2O]_{t=0}$, the mean O_3 concentrations after refill (i.e., the "top" values) as obtained from spectral fitting are listed in column $[O_3]_{top}$, the $^{12}CH_4$ concentrations at the start of the experiments ($t = 0$) as obtained from spectral fitting are listed in column $[^{12}CH_4]_{t=0}$, and the heavy CH_4 concentrations at the start of the experiments ($t = 0$) as obtained from spectral fitting are listed in column $[^xCH_3D]_{t=0}$. Note that, for the experiment including CH_3D, the value of initial concentration only refers to $[^{12}CH_3D]_{t=0}$.

Exp.	Detect.	$^xCH_3D$	T (K)	$[H_2O]_{t=0}$ (hPa)	$[O_3]_{top}$ (hPa)	$[^{12}CH_4]_{t=0}$ (hPa)	$[^xCH_3D]_{t=0}$ (hPa)
1	MCT	CH_3D	298.2 ± 1.2	7.1	–*	0.030	0.054
2	MCT	CH_3D	297.6 ± 0.8	5.6	0.19	0.058	0.042
3	MCT	CH_3D	277.2 ± 0.2	5.2	0.29	0.109	0.046
4	MCT	CH_3D	277.0 ± 0.2	5.1	0.16	0.073	0.035
5	InSb	CH_3D	284.5 ± 0.1	7.2	0.26	0.025	0.033
6	InSb	CH_3D	291.1 ± 0.2	7.4	–*	0.052	0.050
7	InSb	CH_3D	313.5 ± 1.3	7.1	0.17	0.025	0.029
8	InSb	CH_3D	312.4 ± 0.9	4.3	–*	0.022	0.040
9	InSb	$^{13}CH_3D$	298.5 ± 0.1	5.1	–*	0.035	0.026
10	InSb	$^{13}CH_3D$	297.6 ± 0.6	6.4	0.13	0.025	0.033
11	InSb	$^{13}CH_3D$	276.8 ± 0.8	5.4	–*	0.024	0.024
12	InSb	$^{13}CH_3D$	277.2 ± 1.3	5.1	–*	0.022	0.030
13	InSb	$^{13}CH_3D$	287.4 ± 1.2	5.4	–*	0.021	0.028
14	InSb	$^{13}CH_3D$	287.4 ± 0.4	4.5	–*	0.016	0.029
15	InSb	$^{13}CH_3D$	314.4 ± 1.0	5.2	0.26	0.023	0.037
16	InSb	$^{13}CH_3D$	313.8 ± 0.8	8.3	0.17	0.025	0.035

* Spectra recorded during or after photolysis, $[O_3]_{top}$ not available.

slope of $\ln([A]_0/[A]_t)$ versus $\ln([B]_0/[B]_t)$ gives the relative reaction rate coefficient. In these experiments A is $^{12}CH_4$ and B is $^{12}CH_3D$ or $^{13}CH_3D$.

2.2 Photoreactor

Experiments were carried out in the photochemical reactor at the University of Copenhagen, Department of Chemistry. The reactor has been described in detail elsewhere (Nilsson et al., 2009). It consists of a 100 L quartz cell with multipass optics surrounded by 16 UV-C fluorescent Hg lamps in a temperature-controlled housing. The cell is coupled to a Bruker IFS 66v/S FTIR spectrometer with either a mercury cadmium telluride (MCT) (Experiments 1–4) or an indium antimonide (InSb) detector (Experiments 5–16). The InSb detector has a better signal-to-noise ratio; the MCT detector is used in Experiments 1–4 for logistical reasons. Two thermocouple gauges are placed inside the temperature-controlled housing to monitor the temperature and a pressure gauge is connected to the cell to monitor pressure inside the cell. The temperatures and the pressures were logged every 0.5 s.

2.3 Laboratory procedure

Gas mixes were prepared by expanding H_2O vapor (Milli-Q ultrapure water) into the chamber through a glass gas manifold. The two methane isotopologues CH_3D (Experiments 1–8) (purity > 98 %, Cambridge Isotope Laboratories, Inc.) or $^{13}CH_3D$ (Experiments 9–16), and CH_4 (purity > 99 %, Aldrich) and O_3 were flushed into the chamber with a N_2 buffer (purity 99.998 %, Air Liquide), all at the concentrations given in Table 1. $^{13}CH_3D$ was synthesized using the Grignard reaction (see Joelsson et al., 2014). O_3 was generated from O_2 (purity 99.97 %, Air Liquide) using an ozone generator (model AC-20, O_3 Technology), preconcentrated before injection on silica gel cooled with ethanol and dry ice to −67 °C. The desired pressure in the cell (450 hPa) was obtained using N_2 as a bath gas. The starting pressure is chosen such that the pressure is high enough for the N_2 to quench $O(^1D)$ radicals, but low enough to keep the final pressure below atmospheric pressure. The gas mixture was left to rest for up to 1.5 h while several IR spectra were recorded to ensure that no instability or dark chemistry occurs in the gas mix. The UV-C lamps were lit for up to 5 min photolyzing at least 75 % of the O_3 according to

$$O_3 + h\nu \rightarrow O(^1D) + O_2. \quad \text{(R6)}$$

$O(^1D)$ then subsequently reacts with H_2O to yield OH:

$$O(^1D) + H_2O \rightarrow OH + OH. \quad \text{(R7)}$$

Up to 0.2 Pa of O_3 was flushed with about 20 hPa of N_2 into the chamber to compensate for the loss of ozone with time,

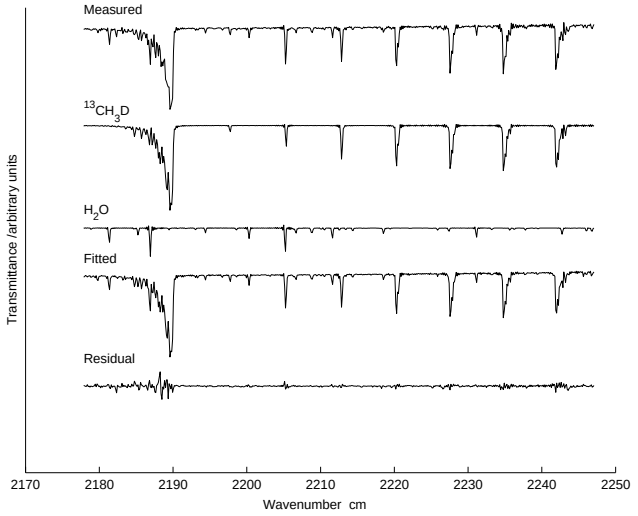

Figure 1. A typical spectral fit in the region where [$^{13}CH_3D$] is obtained (Experiment 10). Experimental data are shown by the topmost line, followed by the fitted (synthetic) partial spectra of the most dominant absorbers ($^{13}CH_3D$ and H_2O), the resulting fitted (synthetic) spectrum (also including CO_2 and CO), and the residual between the measured and fitted spectra.

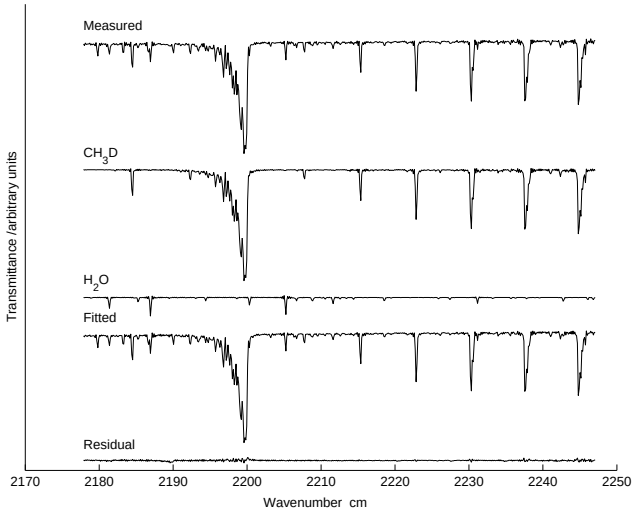

Figure 2. A typical spectral fit in the region where [$^{12}CH_3D$] is obtained (Experiment 5). Experimental data are shown by the topmost line, followed by the fitted (synthetic) partial spectra of the most dominant absorbers (CH_3D and H_2O), the resulting fitted (synthetic) spectrum (also including CO_2 and CO), and the residual between the measured and fitted spectra.

mainly due to $O(^3P) + O_3$. A pressure gradient was established and maintained throughout the filling process such that no gas leaked back from the chamber into the gas line. Spectra were recorded at each filling step. The procedure was repeated until the mix had a final pressure of 933 hPa. Two experiments were conducted at each of the temperatures 278, 288, 298, and 313 K for each of the two heavy methane isotopologues. Exact temperatures are listed in Table 1. After each experiment a dilution test was performed: 133 hPa was pumped out and the chamber is refilled with 133 hPa of N_2. This was repeated 5–6 times. Ideally, concentration calculations from the spectral fits (data analysis described below) of the resulting spectra should give a linear fit with the slope of 1. The slope of these dilution tests is presented in Table 2. In an extra experiment with $^{12}CH_3D$, N_2O (Air Liquide, no purity information available) was added as an $O(^1D)$ tracer. The results from this experiment are used as a benchmark to validate a model that was constructed to investigate the extent of $O(^1D)$ chemistry (see Sect. 2.5). An example of an experimental plot can be found in Fig. 4 and the full data set in Figs. S1–S8 in the Supplement.

2.4 Data analysis

The experimental IR spectra were analyzed using the program MALT, which simulates experimental FTIR spectra (Griffith, 1996) combined with nonlinear least-squares fitting to best-fit the calculated spectra to measured spectra (Griffith et al., 2012). The MALT program generates a simulated spectrum from initial estimates of the absorber concentrations and instrument parameters. The residual between the experimental and simulated spectra is reduced through iteration. Simulated line shapes are generated using HITRAN absorption parameters (version 2008) (Rothman et al., 2009) convolved with an FTIR instrument function simulating the Bruker IFS 66v/S instrument. The InSb detector covers a spectral range from 1800 to 5000 cm^{-1} and the MCT detector covers a spectral range from 400 to 5000 cm^{-1}. The concentrations of $^{12}CH_3D$ and $^{13}CH_3D$ were calculated from spectral fits in the region 2140–2302 cm^{-1} (see Figs. 1 and 2). Interference from H_2O, CO_2, and CO was eliminated by including simulated spectra obtained from the HITRAN database in the fit. As there are no HITRAN data available for $^{13}CH_3D$ in this region, the cross sections from 2000 to 2400 cm^{-1} for this isotopologue were estimated by shifting the spectrum of $^{12}CH_3D$ (see Joelsson et al. (2014)). Concentrations of $^{12}CH_4$ were calculated from spectral fits in the region 2838–2997 cm^{-1}. Interference from $^{13}CH_3D$ was reduced by including temperature-adjusted reference spectra in the fit, and interference from $^{12}CH_3D$, H_2O, and H_2CO was by including simulated spectra obtained from the HITRAN database in the fit (see Fig. 3). The spectral windows were sometimes adjusted to exclude saturated lines.

After [$^xCH_3D$] (where $x = 12$ or $x = 13$) and [$^{12}CH_4$] were obtained from the spectral analysis, $\ln([^xCH_3D]_0/[^xCH_3D]_t)$ was plotted against $\ln([^{12}CH_4]_0/[^{12}CH_4]_t)$ as described in Sect. 2.1. A straight line was fitted to these data points using a weighted total least-squares routine (York et al., 2004). The fitting procedure takes uncertainties in both dimensions into account. The uncertainty $\sigma(\ln([A]_0/[A]_t))$ was calculated

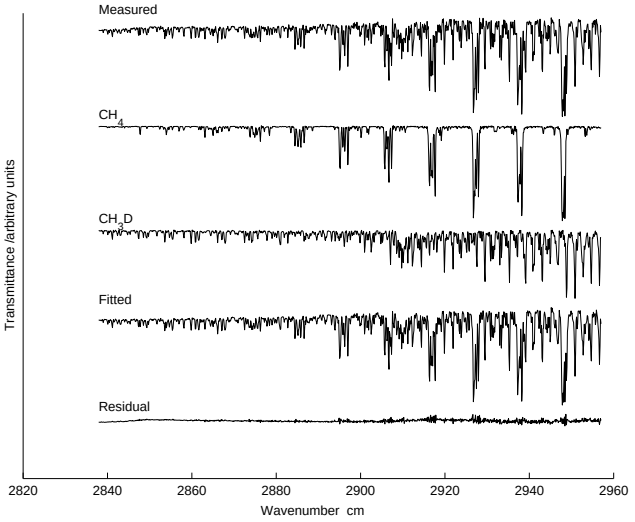

Figure 3. A typical spectral fit in the region where $[^{12}CH_4]$ is obtained (Experiment 5). Experimental data are shown by the topmost line, followed by the fitted partial (synthetic) spectra of the most dominant absorbers (CH_4 and CH_3D), the resulting fitted (synthetic) spectrum (also including H_2O), and the residual between the measured and fitted spectra.

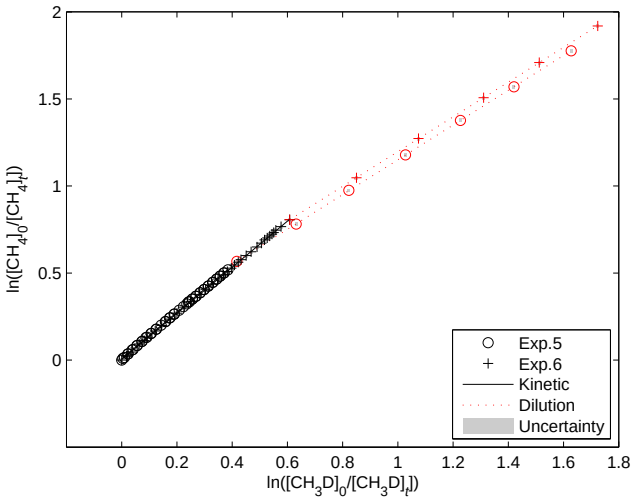

Figure 4. A typical experimental outcome, Experiment 5 and 6: CH_3D, $T = 288$ K. Experimental data are shown using black open circles (Exp. 5) and black plus signs (Exp. 6). Corresponding dilution test points are shown using red symbols. A linear fit of the experimental points is shown using a black solid line, linear fits of the subsequent dilution test are represented by a red dotted line, and uncertainties for each point are represented by gray areas.

using standard error propagation:

$$\sigma\left(\ln([A]_0/[A]_t)\right) = \sqrt{\left(\frac{\sigma([A]_0)}{[A]_0}\right)^2 + \left(\frac{\sigma([A]_t)}{[A]_t}\right)^2}, \quad (5)$$

where $\sigma([A])$ was obtained as output from MALT. The fitting procedure, performed using a MATLAB script (York et al., 2004), also yields an error estimation which is defined as the uncertainty of the kinetic isotope effect $\sigma(\alpha)$. An example of a straight line fit can be found in Fig. 4 and the full data set in Figs. S1–S8 in the Supplement. In the temperature dependence curve fitting procedure, the parameters A and B are from a linearized version of the Arrhenius equation:

$$\ln(k) = \ln(A) + B \cdot T^{-1}, \quad (6)$$

which is fitted to the experimental data. Also here, the method of York et al. (2004) was used. The temperature in the cell was taken as the spatial average of the measurements from two thermocouples inside the temperature housing. The experiment temperature was defined by the temporal mean of the spatially averaged temperature measurement series and the uncertainty of the experiment temperature was the standard deviation of the spatially averaged temperature measurement series.

2.5 Kinetic model

A kinetic model was used to determine the influence of $O(^1D)$, Reaction (R3), which rivals Reaction (R1). The model has been previously described and was used by Nilsson et al. (2012). However, only the methane reaction subset and associated (O_x and HO_x) chemistry were used here. The Kintecus program (Ianni, 2003) simulates the photolysis of O_3 and the following oxidation chain of CH_4. To model ozone photolysis accurately, the modeled O_3 was matched to the measured value by adjusting the photolysis rate, then the model was verified by comparing the decrease in CH_4 and the increase in H_2O during the experiment. The model was run for each refill of O_3, where the reaction rates of Reactions (R1) and (R3) were obtained. The model was designed for room temperature; experiments at other temperatures were not modeled. Experiment 2 was thus modeled: 4.4 % of CH_4 was estimated to be lost to Reaction (R3). In an additional experiment, N_2O was introduced into the chamber as an $O(^1D)$ tracer. Since N_2O does not react with OH and is not photolyzed at the wavelengths present (Nilsson et al., 2009), the decrease in N_2O should be only due to Reaction (R8):

$$N_2O + O(^1D) \rightarrow \text{products}. \quad (R8)$$

The amount of CH_4 lost by Reaction (R3) can therefore be approximated by

$$1 - \frac{[CH_4]_t}{[CH_4]_0} = 1 - \exp\left(-k_{R3}[O(^1D)]t\right) = 1 - \frac{[N_2O]_t}{[N_2O]_0}^{(k_{R8}/k_{R3})}, \quad (7)$$

where $k_{R8} = 1.27 \times 10^{-10}\,\mathrm{cm^{-3}\,s^{-1}}$ and $k_{R3} = 1.75 \times 10^{-10}\,\mathrm{cm^{-3}\,s^{-1}}$ (Sander et al., 2011). This gives

Table 2. Results. The experiment numbers are listed in column Exp., the heavy CH_4 isotopologue included in the experiments is listed in column $^xCH_3D$, the mean measured temperatures in the photoreactor are listed in column T, the kinetic isotope effect corresponding to the isotopologue is listed in column α, and the result of the dilution experiments is listed in column k_{dil}.

Exp.	$^xCH_3D$	T (K)	α	k_{dil}
1	CH_3D	298.2 ± 1.2	1.302 ± 0.038	1.011 ± 0.048
2	CH_3D	297.6 ± 0.8	1.314 ± 0.020	–*
3	CH_3D	277.2 ± 0.2	1.294 ± 0.017	0.962 ± 0.037
4	CH_3D	277.0 ± 0.2	1.335 ± 0.017	–*
5	CH_3D	284.5 ± 0.1	1.334 ± 0.012	0.999 ± 0.009
6	CH_3D	291.1 ± 0.2	1.323 ± 0.010	0.998 ± 0.010
7	CH_3D	313.5 ± 1.3	1.301 ± 0.007	1.006 ± 0.031
8	CH_3D	312.4 ± 0.9	1.338 ± 0.010	–*
9	$^{13}CH_3D$	298.5 ± 0.1	1.359 ± 0.022	1.000 ± 0.029
10	$^{13}CH_3D$	297.6 ± 0.6	1.314 ± 0.007	0.990 ± 0.064
11	$^{13}CH_3D$	276.8 ± 0.8	1.357 ± 0.046	1.016 ± 0.031
12	$^{13}CH_3D$	277.2 ± 1.3	1.344 ± 0.013	1.008 ± 0.030
13	$^{13}CH_3D$	287.4 ± 1.2	1.346 ± 0.025	1.009 ± 0.022
14	$^{13}CH_3D$	287.4 ± 0.4	1.342 ± 0.015	1.011 ± 0.019
15	$^{13}CH_3D$	314.4 ± 1.0	1.316 ± 0.016	1.003 ± 0.038
16	$^{13}CH_3D$	313.8 ± 0.8	1.331 ± 0.033	1.001 ± 0.034

* No dilution test performed.

2.3 % [CH_4] lost by oxidation of $O(^1D)$, Reaction (R3). The kinetic model described above estimated that 4.7 % [CH_4] was lost by Reaction (R3) for this additional experiment. Both methods agree that $O(^1D)$ loss is a minor channel. No correction is applied, and the possible deviation is included in the estimated error.

3 Theoretical procedure

Rate constants and kinetic isotope effects for $CH_4 + OH$ were calculated using a procedure similar to that employed by Joelsson et al. (2014).

3.1 Computational chemistry calculations

The geometries of reactants, products, and transition states were determined using a geometry optimization procedure based on the unrestricted MP2 method (Møller and Plesset, 1934) and the aug-cc-pVQZ orbital basis set (Dunning Jr., 1989; Woon and Dunning Jr., 1993). Harmonic vibrational frequencies for all relevant isotopologues of reactants, products, and transition states were obtained at the same level of theory. The calculations were carried out using the Gaussian 09 program package (Frisch et al., 2009).

The electronic energy of the optimized structures were refined using the CCSD(T) method (Watts et al., 1993; Knowles et al., 1993, 2000) with aug-cc-pVTZ, aug-cc-pVQZ, and aug-cc-pV5Z basis sets. The results from the different basis sets were used to extrapolate the electronic energy at the complete basis set limit following the approach of Halkier et al. (1998) as described by Joelsson et al. (2014).

3.2 Rate constant calculations

The abstraction of a CH_4 hydrogen atom by OH can occur at four different sites. Depending on the methane isotopologue in question, these sites are either distinguishable or indistinguishable. Microscopic rate constants are calculated for hydrogen abstraction at each site using classical transition state theory with a tunneling correction factor,

$$k^{(i)}_{micro} = \eta^{(i)}_{tun} \frac{k_b T}{h} \frac{Q^{(i)}_{TS}}{Q_{reac}} \exp(-\Delta E^{(i)}/RT), \quad (8)$$

where $\Delta E^{(i)}$ is the reaction barrier height (including the zero-point vibrational energy) for the ith reaction path. $\eta^{(i)}_{tun}$ is a tunneling correction factor obtained using the Wigner tunneling correction (Wigner, 1932). $Q^{(i)}_{TS}$ and Q_{reac} are the partition functions for the transition state and reacting pair, respectively. The total rate constant is obtained by summing over the microscopic rate constants.

4 Results and discussion

The results of the 16 individual experiments (eight for each isotopologue) are tabulated in Table 2. The resulting $^D\alpha$, $^{13C}\alpha$, and $^{13C,D}\alpha$ values from the experimental and theoretical studies are tabulated in Tables 3, 4, and 5 along with previous experimental and theoretical results. The results are also shown in Figs. 5 and 6 for reactions of CH_3D and $^{13}CH_3D$, respectively.

The exponential curve fits yielded the parameters presented in Tables 3 and 5 giving $^D\alpha_{Arr} = 1.32 \pm 0.13$ and $^{13C,D}\alpha_{Arr} = 1.32 \pm 0.20$ at $T = 298$ K. The mean of results of room temperature experiments Experiments 1 and 2 and Experiments 9 and 10 is $^D\alpha_{exp} = 1.31 \pm 0.01$ and $^{13C,D}\alpha_{exp} = 1.34 \pm 0.03$, respectively. It follows that $\gamma_{exp} = 1.02 \pm 0.02$ at $T = 298$ K, using $^{13C}\alpha_{exp} = 1.0039 \pm 0.0002$ (Saueressig et al., 2001), meaning that the clumped isotope might react slower relative to what would be predicted based on the kinetic isotope effects of CH_3D and $^{13}CH_4$. However, if the Arrhenius parameters are used to calculate the kinetic isotope effects at $T = 298$ K, $\gamma_{Arr} = 1.00 \pm 0.18$ (i.e., the reaction has no clumping effect). All uncertainties are given as 1 standard deviation (σ). The theoretical results give $\gamma_{theory} = 1.00$ at $T = 298$ K.

The present experimental room temperature results for $^D\alpha$ agree, to within the error bars, with the previous experimental studies, with the exception of DeMore (1993). DeMore (1993) used FTIR spectroscopy with a slow flow setup where the two methane isotopologues were measured separately with a common reference compound. The low $^D\alpha$ value in DeMore (1993) may be explained by interference from

Table 3. Experimental and theoretical studies of $^{D}\alpha$. The temperature dependence studies are presented in the Arrhenius form $^{D}\alpha(T) = A(T/298\,\mathrm{K})^{n}\exp(BT^{-1})$, where A, n, and B are tabulated; T is the given temperature range; and $^{D}\alpha(T = 298\,\mathrm{K})$ is the resulting kinetic isotope effect at $T = 298$ K. Where no B coefficient is presented, A can be taken as $^{D}\alpha(T)$ for the given temperature range. All uncertainties are given as 1 standard deviation (σ).

Study	A	n	B (K)	T (K)	$^{D}\alpha(T = 298\,\mathrm{K})$
Experimental studies					
Present study[a]	1.23 ± 0.08	0	21 ± 21	[278, 313]	1.31 ± 0.01[h]
Saueressig et al. (2001) [b]	1.294 ± 0.009	–	–	296	–
Gierczak et al. (1997) [c]	1.09 ± 0.05	0	49 ± 11	[220, 415]	1.25 ± 0.07
DeMore (1993) [a]	0.91	0	75	[298, 360]	1.17
Gordon and Mulac (1975) [d]	1.50	–	–	416	–
Gordon and Mulac (1975) [d,i]	1.06	–	–	416	–
Theoretical studies					
Present study[e]	1.314	0	6.354	[200, 300]	1.339
Sellevåg et al. (2006) [f]	[1.30, 1.00]	–	–	[200, 1500]	1.27
Masgrau et al. (2001) [g,j]	1.00	−0.02	50.5	[200, 1500]	1.25

[a] Fourier transform infrared spectroscopy – relative rate. [b] Tunable diode laser absorption spectroscopy–isotope ratio mass spectrometry. [c] Pulsed photolysis–pulsed laser-induced fluorescence. [d] Pulse radiolysis. [e] Transition state theory with Wigner tunneling correction. [f] Canonical unified statistical theory. [g] Multicoefficient correlation method. [h] Average room temperature value, not obtained from curve fit. [i] Re-evaluated by DeMore (1993). [j] Arrhenius parameters available at NIST (2015).

Table 4. Experimental and theoretical studies of $^{13}C\alpha$. The temperature dependence studies are presented in the Arrhenius form $^{13}C\alpha(T) = A\exp(BT^{-1})$, where A and B are tabulated, T is the given temperature range, and $^{13}C\alpha(T = 298\,\mathrm{K})$ is the resulting kinetic isotope effect at $T = 298$ K. Where no B coefficient is presented, A can be taken as $^{13}C\alpha(T)$ for the given temperature range. All uncertainties are given as 1 standard deviation (σ).

Study	A	B (K)	T (K)	$^{13}C\alpha(T = 298\,\mathrm{K})$
Experimental studies				
Saueressig et al. (2001) [a]	1.0039 ± 0.0002	–	296	–
Cantrell et al. (1990) [b]	1.0054 ± 0.0005	–	[273, 353]	1.0054 ± 0.0005
Rust and Stevens (1980) [c,i]	1.003	–	–	–
Theoretical studies				
Present study[d]	1.0137	−1.219	[200, 300]	1.0094
Sellevåg et al. (2006) [e]	[1.014, 1.00]	–	[200, 1500]	1.003
Gupta et al. (1997) [f]	1.010	–	300	–
Melissas and Truhlar (1993) [g,h]	[1.005, 1.001]	–	[223, 416]	1.005
Lasaga and Gibbs (1991) [h]	[1.0036, 1.0076]	–	[150, 350]	–

[a] Tunable diode laser absorption spectroscopy–isotope ratio mass spectrometry. [b] Gas chromatography–mass spectrometry. [c] Isotope ratio mass spectrometry. [d] Transition state theory with Wigner tunneling correction. [e] Canonical variational transition state theory. [f] Conventional transition state theory. [g] Interpolated variational transition state theory with centrifugal-dominant, small-curvature tunneling coefficients. [h] Ab initio calculations. [i] No temperature information available.

$O(^1D)$ radicals: OH radicals were produced by photolysis of O_3 at 254 nm in the presence of H_2O, as in the present study. A relatively high rate of Reaction (R3) would reduce the final kinetic isotope effect, since the kinetic isotope effect for oxidation with $O(^1D)$ is smaller than the kinetic isotope effect for the oxidation of OH (Saueressig et al., 2001). The present experimental results of $^{D}\alpha$ are also in good agreement with Masgrau et al. (2001) and Sellevåg et al. (2006). The theoretical calculations of $^{D}\alpha$ give a slightly higher value than the experimental results, although they are in good agreement with the best Arrhenius curve fit at $T = 298$ K.

The experimental room temperature result for $^{13C,D}\alpha = 1.34 \pm 0.03$ agrees, to within the error bar, with both the theoretical value and the best estimate of the Arrhenius curve fit at $T = 298$ K.

The theoretical calculations show a very small temperature dependence; the variability in the experimental data is large compared to the value of the slope, making a quantification of the temperature dependence uncertain. Furthermore, the

Table 5. Experimental and theoretical studies of $^{13C,D}\alpha$. The temperature dependencies are presented in the Arrhenius form $^{13C,D}\alpha(T) = A\exp(BT^{-1})$, where A and B are tabulated, T is the given temperature range, and $^{13C,D}\alpha(T = 298\,\mathrm{K})$ is the resulting kinetic isotope effect at $T = 298$ K. All uncertainties are given as 1 standard deviation (σ).

Study	A	B (K)	T (K)	$^{13C,D}\alpha(T = 298\,\mathrm{K})$
Experimental study[a]	1.18 ± 0.10	38 ± 26	[278, 313]	1.34 ± 0.03[c]
Theoretical study[b]	1.328	5.301	[200, 300]	1.349

[a] Fourier transform infrared spectroscopy – relative rate. [b] Transition state theory with Wigner tunneling correction. [c] Average room temperature value, not obtained from curve fit.

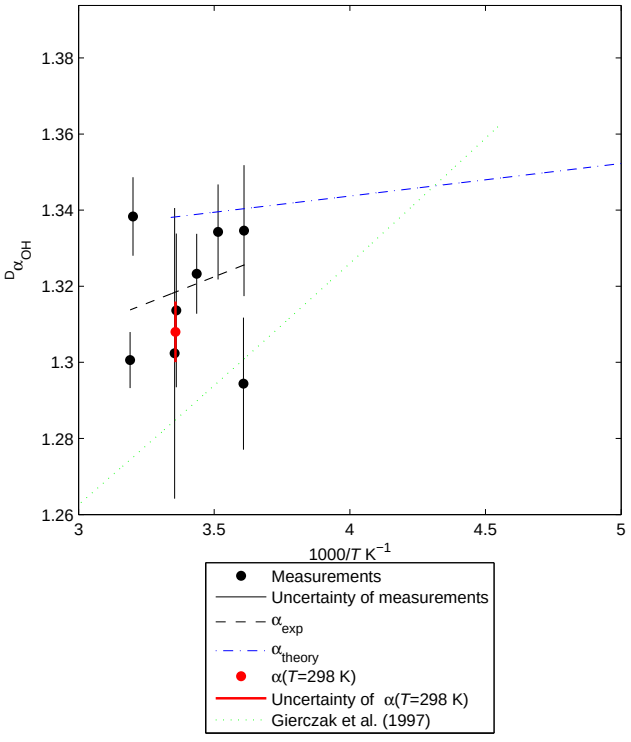

Figure 5. The individual measurements of $^{D}\alpha$ are represented by black points, the accompanying individual error bars are represented by thin black solid lines, the experimental Arrhenius curve fit is represented by a black dashed line, the theoretical Arrhenius curve fit is represented by a blue dashed-dotted line, the mean of the room temperature measurements is represented by a red solid circle, the uncertainty of the room temperature measurements is represented by a thick red solid line, and the result from Gierczak et al. (1997) (which is included for comparison) is represented by a green dotted line. All uncertainties are given as 1 standard deviation (σ).

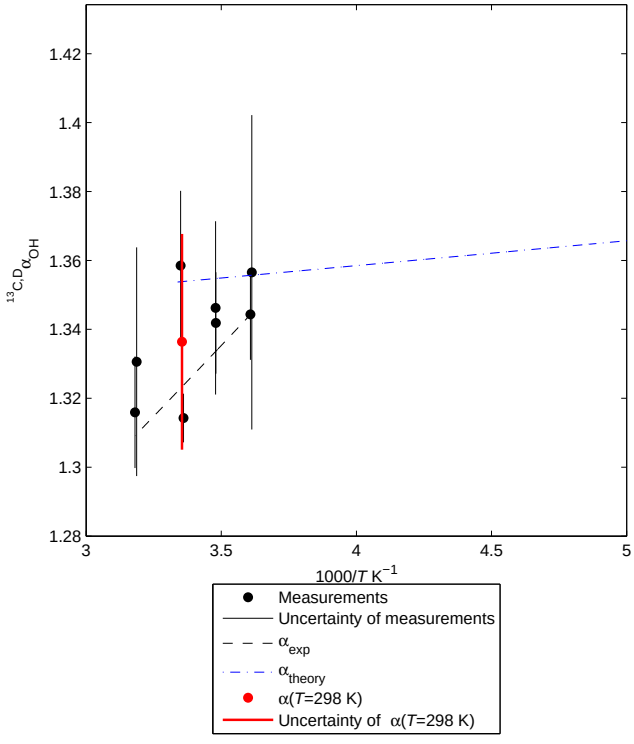

Figure 6. The individual measurements of $^{13C,D}\alpha$ are represented by black points, the accompanying individual error bars are represented by thin black solid lines, the experimental Arrhenius curve fit is represented by a black dashed line, the theoretical Arrhenius curve fit is represented by a blue dashed-dotted line, the mean of the room temperature measurements is represented by a red solid circle, and the uncertainty of the room temperature measurements is represented by a thick red solid line. All uncertainties are given as 1 standard deviation (σ).

theoretical analysis revealed that the primary cause for the kinetic isotope effect is the substantially reduced reactivity of the D atom, which, in turn, can be explained by a significant increase in reaction barrier due to changes in vibrational zero-point energy and to a lesser extent tunneling.

Atmospheric implications

At steady state, assuming no clumping in emissions, $\Delta(^{13}CH_3D) = \ln(\gamma)$. It follows that $\Delta(^{13}CH_3D) = 0.02 \pm 0.02$, implying that the clumped isotope effect of the OH reaction is small. Wang et al. (2015) studied a variety of natural samples and found $\Delta(^{13}CH_3D)$ values that vary from (-3.36 ± 1.42)‰ for samples of bubbling gases from The

Cedars, Cazadero, California, USA, to (6.17 ± 0.34)‰ for samples from gas voids and hydrates in sediment cores from the northern Cascadia margin. Methanogenic bacteria in the laboratory ranged from -1.34 to 2.29 ‰. Natural gas was found to vary from 2.53 to 5.18 ‰. Given these natural variations in $\Delta(^{13}CH_3D)$ values of the sources, it is clear from isotopic mass balance that the fractionation from atmospheric oxidation by OH will likely have little effect on the observed $\Delta(^{13}CH_3D)$ value of tropospheric methane. Rather, this number will reflect the relative contributions of the sources. $\Delta(^{13}CH_3D)$ would therefore be a more straightforward tracer for tracking methane sources than conventional isotopic analysis. Further field studies are clearly needed to characterize $\Delta(^{13}CH_3D)$ values of microbial and thermal methane.

5 Conclusions

We present experimentally derived $CH_4 + OH$ kinetic isotope effects and their temperature dependence for CH_3D and $^{13}CH_3D$; the latter is reported for the first time. We find $^{D}\alpha = 1.31 \pm 0.01$ and $^{13C,D}\alpha = 1.34 \pm 0.03$ at room temperature, implying that the kinetic isotope effect is multiplicative such that $(k_{CH_4}/k_{^{13}CH_4})(k_{CH_4}/k_{CH_3D}) = k_{CH_4}/k_{^{13}CH_3D}$ to within the experimental uncertainty. We compare our experimental results to theoretical estimates derived using transition state theory with tunneling correction and kinetic isotope effects reported in the literature. We find good agreement between theoretical and literature values. Based on these experiments we find that the OH reaction (the main sink of methane) at steady state has a clumped $\Delta(^{13}CH_3D) = 0.02 \pm 0.02$.

The Supplement related to this article is available online at doi:10.5194/acp-16-4439-2016-supplement.

Acknowledgements. This research received funding from the European Community's Seventh Framework Programme (FP7/2007-2013) under grant agreement no. 237890, the Carlsberg foundation, and the Danish Council for Independent Research.

Edited by: E. Harris

References

Allan, W., Lowe, D., and Cainey, J.: Active chlorine in the remote marine boundary layer: Modeling anomalous measurements of $\delta^{13}C$ in methane, Geophys. Res. Lett., 28, 3239–3242, 2001a.

Allan, W., Manning, M., Lassey, K., Lowe, D., and Gomez, A.: Modeling the variation of δ13C in atmospheric methane: Phase ellipses and the kinetic isotope effect, Global Biogeochem. Cy., 15, 467–481, 2001b.

Bergamaschi, P., Bräunlich, M., Marik, T., and Brenninkmeijer, C. A.: Measurements of the carbon and hydrogen isotopes of atmospheric methane at Izaña, Tenerife: Seasonal cycles and synoptic-scale variations, J. Geophys. Res.-Atmos., 105, 14531–14546, 2000.

Cantrell, C., Shetter, R., Mcdaniel, A., Calvert, J., Davidson, J., Lowe, D., Tyler, S., Cicerone, R., and Greenberg, J.: Carbon Kinetic Isotope Effect in the Oxidation of Methane by the Hydroxyl Radical, J. Geophys. Res., 95, 22455–22462, 1990.

Ciais, P., Sabine, C., Bala, G., Bopp, L., Brovkin, V., Canadell, J., Chhabra, A., DeFries, R., Galloway, J., Heimann, M., Jones, C., Le Quéré, C., Myneni, R., Piao, S., and Thornton, P.: Carbon and Other Biogeochemical Cycles, in: Climate Change 2013: The Physical Science Basis. Contribution of Working Group I to the Fifth Assessment Report of the Intergovernmental Panel on Climate Change, Cambridge University Press, Cambridge, United Kingdom and New York, NY, USA, 2013.

Crowley, J. N., Saueressig, G., Bergamaschi, P., Fischer, H., and Harris, G. W.: Carbon kinetic isotope effect in the reaction $CH_4 + Cl$: a relative rate study using FTIR spectroscopy, Chem. Phys. Lett., 303, 268–274, 1999.

DeMore, W.: Rate constant ratio for the reactions of OH with CH_3D and CH_4, J. Phys. Chem., 97, 8564–8566, 1993.

Dunning Jr., T. H.: Gaussian basis sets for use in correlated molecular calculations. I. The atoms boron through neon and hydrogen, J. Chem. Phys., 90, 1007–1023, 1989.

Eiler, J. M., Clog, M., Magyar, P., Piasecki, A., Sessions, A., Stolper, D., Deerberg, M., Schlueter, H. J., and Schwieters, J.: A high-resolution gas-source isotope ratio mass spectrometer, Int. J. Mass Spectrom., 335, 45–56, 2013.

Feilberg, K. L., Griffith, D. W. T., Johnson, M. S., and Nielsen, C. J.: The ^{13}C and D kinetic isotope effects in the reaction of CH_4 with Cl, Int. J. Chem. Kinet., 37, 110–118, 2005.

Ferretti, D. F., Miller, J. B., White, J. W. C., Etheridge, D. M., Lassey, K. R., Lowe, D. C., Meure, C. M. M., Dreier, M. F., Trudinger, C. M., van Ommen, T. D., and Langenfelds, R. L.: Unexpected changes to the global methane budget over the past 2000 years, Science, 309, 1714–1717, 2005.

Frisch, M. J., Trucks, G. W., Schlegel, H. B., Scuseria, G. E., Robb, M. A., Cheeseman, J. R., Scalmani, G., Barone, V., Mennucci, B., Petersson, G. A., Nakatsuji, H., Caricato, M., Li, X., Hratchian, H. P., Izmaylov, A. F., Bloino, J., Zheng, G., Sonnenberg, J. L., Hada, M., Ehara, M., Toyota, K., Fukuda, R., Hasegawa, J., Ishida, M., Nakajima, T., Honda, Y., Kitao, O., Nakai, H., Vreven, T., Montgomery Jr., J. A., Peralta, J. E., Ogliaro, F., Bearpark, M., Heyd, J. J., Brothers, E., Kudin, K. N., Staroverov, V. N., Kobayashi, R., Normand, J., Raghavachari, K., Rendell, A., Burant, J. C., Iyengar, S. S., Tomasi, J., Cossi, M., Rega, N., Millam, J. M., Klene, M., Knox, J. E., Cross, J. B., Bakken, V., Adamo, C., Jaramillo, J., Gomperts, R., Stratmann, R. E., Yazyev, O., Austin, A. J., Cammi, R., Pomelli, C., Ochterski, J. W., Martin, R. L., Morokuma, K., Zakrzewski, V. G., Voth, G. A., Salvador, P., Dannenberg, J. J., Dapprich, S., Daniels, A. D., Farkas, O., Foresman, J. B., Ortiz, J. V., Cioslowski, J., and Fox, D. J.: Gaussian 09 Revision A.1, Gaussian Inc., Wallingford CT, 2009.

Gierczak, T., Talukdar, R. K., Herndon, S. C., Vaghjiani, G. L., and Ravishankara, A. R.: Rate Coefficients for the Reactions of Hy-

droxyl Radicals with Methane and Deuterated Methanes, J. Phys. Chem. A, 101, 3125–3134, 1997.

Gordon, S. and Mulac, W. A.: Reaction of OH(X2-PI) radical produced by pulse-radiolysis of water-vapor, Int. J. Chem. Kinet., 1, 289–299, 1975.

Griffith, D. W. T., Deutscher, N. M., Caldow, C., Kettlewell, G., Riggenbach, M., and Hammer, S.: A Fourier transform infrared trace gas and isotope analyser for atmospheric applications, Atmos. Meas. Tech., 5, 2481–2498, doi:10.5194/amt-5-2481-2012, 2012.

Griffith, D. W. T.: Synthetic Calibration and Quantitative Analysis of Gas-Phase FT-IR Spectra, Appl. Spectrosc., 50, 59–70, 1996.

Gupta, M. L., McGrath, M. P., Cicerone, R. J., Rowland, F. S., and Wolfsberg, M.: C-12/C-13 kinetic isotope effects in the reactions of CH_4 with OH and Cl, Geophys. Res. Lett., 24, 2761–2764, 1997.

Halkier, A. T. H., Jørgensen, P., Klopper, W., Koch, H., Olsen, J., and Wilson, A. K.: Basis-set convergence in correlated calculations on Ne, N_2, and H_2O, Chem. Phys. Lett., 286, 243–252, 1998.

Ianni, J.: A Comparison of the Bader-Deuflhard and the Cash-Karp Runge-Kutta Integrators for the GRI-MECH 3.0 Model Base on the Chemical Kinetics Code Kintecus, Computational Fluid and Solid Mechanics, 1368–1372, Elsevier Science Ltd., Oxford, UK, 2003.

IPCC: Climate Change 2013: The Physical Science Basis. Contribution of Working Group I to the Fifth Assessment Report of the Intergovernmental Panel on Climate Change, Cambridge University Press, Cambridge, United Kingdom and New York, NY, USA, 2013.

Joelsson, L. M. T., Forecast, R., Schmidt, J. A., Meusinger, C., Nilsson, E. J. K., Ono, S., and Johnson, M. S.: Relative rate study of the kinetic isotope effect in the (CH_3D)-C-13 + Cl reaction, Chem. Phys. Lett., 605, 152–157, 2014.

Kirschke, S., Bousquet, P., Ciais, P., Saunois, M., Canadell, J. G., Dlugokencky, E. J., Bergamaschi, P., Bergmann, D., Blake, D. R., Bruhwiler, L., Cameron-Smith, P., Castaldi, S., Chevallier, F., Feng, L., Fraser, A., Heimann, M., Hodson, E. L., Houweling, S., Josse, B., Fraser, P. J., Krummel, P. B., Lamarque, J.-F., Langenfelds, R. L., Le Quéré, C., Naik, V., O'Doherty, S., Palmer, P. I., Pison, I., Plummer, D., Poulter, B., Prinn, R. G., Rigby, M., Ringeval, B., Santini, M., Schmidt, M., Shindell, D. T., Simpson, I. J., Spahni, R., Steele, L. P., Strode, S. A., Sudo, K., Szopa, S., van der Werf, G. R., Voulgarakis, A., van Weele, M., Weiss, R. F., Williams, J. E., and Zeng, G.: Three decades of global methane sources and sinks, Nat. Geosci., 6, 813–823, 2013.

Knowles, P. J., Hampel, C., and Werner, H.-J.: Coupled cluster theory for high spin, open shell reference wave functions, J. Chem. Phys., 99, 5219–5227, 1993.

Knowles, P. J., Hampel, C., and Werner, H.-J.: Erratum: "Coupled cluster theory for high spin, open shell reference wave functions" [J. Chem. Phys. 99, 5219 (1993)], J. Chem. Phys., 112, 3106–3107, 2000.

Lasaga, A. C. and Gibbs, G.: Ab initio studies of the kinetic isotope effect of the $CH_4 + OH\bullet$ atmospheric reaction, Geophys. Res. Lett., 18, 1217–1220, 1991.

Lassey, K. R., Etheridge, D. M., Lowe, D. C., Smith, A. M., and Ferretti, D. F.: Centennial evolution of the atmospheric methane budget: what do the carbon isotopes tell us?, Atmos. Chem. Phys., 7, 2119–2139, doi:10.5194/acp-7-2119-2007, 2007.

Liu, Q. and Liu, Y.: Clumped-isotope signatures at equilibrium of CH_4, NH_3, H_2O, H_2S and SO_2, Geochim. Cosmochim. Ac., 175, 252–270, 2016.

Lowe, D. C., Manning, M. R., Brailsford, G. W., and Bromley, A. M.: The 1991–1992 atmospheric methane anomaly: Southern Hemisphere C-13 decrease and growth rate fluctuations, Geophys. Res. Lett., 24, 857–860, 1997.

Ma, Q., Wu, S., and Tang, Y.: Formation and abundance of doubly-substituted methane isotopologues ((CH_3D)-C-13) in natural gas systems, Geochim. Cosmochim. Ac., 72, 5446–5456, 2008.

Masgrau, L., Gonzalez-Lafont, A., and Lluch, J. M.: The reactions $CH_nD_{4-n} + OH \rightarrow P$ and $CH_4 + OD \rightarrow CH_3 + HOD$ as a test of current direct dynamics multicoefficient methods to determine variational transition state rate constants. II, J. Chem. Phys., 115, 4515–4526, 2001.

Melissas, V. S. and Truhlar, D. G.: Deuterium and C-13 kinetic isotope effects for the reaction of OH with CH_4, J. Chem. Phys., 99, 3542–3552, 1993.

Møller, C. and Plesset, M. S.: Note on an Approximation Treatment for Many-Electron Systems, Phys. Rev., 46, 618–622, 1934.

Nilsson, E. J. K., Eskebjerg, C., and Johnson, M. S.: A photochemical reactor for studies of atmospheric chemistry, Atmos. Environ., 43, 3029–3033, 2009.

Nilsson, E. J. K., Andersen, V. F., Nielsen, O. J., and Johnson, M. S.: Rate coefficients for the chemical reactions of CH_2F_2, $CHClF_2$, CH_2FCF_3 and CH_3CCl_3 with $O(^1D)$ at 298 K, Chem. Phys. Lett., 554, 27–32, 2012.

NIST: National Institute of Standards and Technology Chemical Kinetics Database, available at: http://kinetics.nist.gov (last access: 2 October 2015), 2015.

Ono, S., Wang, D. T., Gruen, D. S., Sherwood Lollar, B., Zahniser, M. S., McManus, B. J., and Nelson, D. D.: Measurement of a Doubly Substituted Methane Isotopologue, $^{13}CH_3D$, by Tunable Infrared Laser Direct Absorption Spectroscopy, Anal. Chem., 86, 6487–6494, 2014.

Pohlman, J., Kaneko, M., Heuer, V., Coffin, R., and Whiticar, M.: Methane sources and production in the northern Cascadia margin gas hydrate system, Earth Planet. Sc. Lett., 287, 504–512, 2009.

Quay, P., Stutsman, J., Wilbur, D., Snover, A., Dlugokencky, E., and Brown, T.: The isotopic composition of atmospheric methane, Global Biogeochem. Cy., 13, 445–461, 1999.

Rothman, L. S., Gordon, I. E., Barbe, A., Benner, Bernath, P. F., Birk, M., Boudon, V., Brown, L. R., Campargue, A., and Champion, J. P.: The HITRAN 2008 molecular spectroscopic database, J. Quant. Spectrosc. Ra., 110, 533–572, 2009.

Rust, F. and Stevens, C.: Carbon kinetic isotope effect in the oxidation of methane by hydroxyl, Int. J. Chem. Kinet., 12, 371–377, 1980.

Sander, S. P., Friedl, R., Barker, J., Golden, D., Kurylo, G., Wine, P., Abbatt, J., Burkholder, J., Kolb, C., Moortgat, G., Huie, R. E., and Orkin, V. L.: Chemical kinetics and photochemical data for use in atmospheric studies: evaluation number 17, National Aeronautics and Space Administration, Jet Propulsion Laboratory, California Institute of Technology Pasadena, CA, 2011.

Saueressig, G., Bergamaschi, P., Crowley, J. N., Fischer, H., and Harris, G. W.: Carbon kinetic isotope effect in the reaction of CH_4 with Cl atoms, Geophys. Res. Lett., 22, 1225–1228, 1995.

Saueressig, G., Bergamaschi, P., Crowley, J. N., Fischer, H., and Harris, G. W.: D/H kinetic isotope effect in the reaction CH_4+Cl, Geophys. Res. Lett., 23, 3619–3622, 1996.

Saueressig, G., Crowley, J. N., Bergamaschi, P., Bruhl, C., Brenninkmeijer, C. A. M., and Fischer, H.: Carbon 13 and D kinetic isotope effects in the reactions of CH_4 with O(D-1) and OH: New laboratory measurements and their implications for the isotopic composition of stratospheric methane, J. Geophys. Res.-Atmos., 106, 23127–23138, 2001.

Schmidt, J. A. and Johnson, M. S.: Clumped isotope perturbation in tropospheric nitrous oxide from stratospheric photolysis, Geophys. Res. Lett., 42, 3546–3552, 2015.

Schmidt, J. A., Johnson, M. S., and Schinke, R.: Carbon dioxide photolysis from 150 to 210 nm: Singlet and triplet channel dynamics, UV-spectrum, and isotope effects, P. Natl. Acad. Sci., 110, 17691–17696, 2013.

Sellevåg, S. R., Nyman, G., and Nielsen, C. J.: Study of the carbon-13 and deuterium kinetic isotope effects in the Cl and OH reactions of CH_4 and CH_3Cl, J. Phys. Chem. A, 110, 141–152, 2006.

Stolper, D. A., Sessions, A. L., Ferreira, A. A., Santos Neto, E. V., Schimmelmann, A., Shusta, S. S., Valentine, D. L., and Eiler, J. M.: Combined C-13-D and D-D clumping in methane: Methods and preliminary results, Geochim. Cosmochim. Ac., 126, 169–191, 2014.

Tyler, S. C., Rice, A. L., and Ajie, H. O.: Stable isotope ratios in atmospheric CH_4: Implications for seasonal sources and sinks, J. Geophys. Res.-Atmos., 112, D03303, doi:10.1029/2006JD007231, 2007.

Wang, D. T., Gruen, D. S., Lollar, B. S., Hinrichs, K.-U., Stewart, L. C., Holden, J. F., Hristov, A. N., Pohlman, J. W., Morrill, P. L., Koenneke, M., Delwiche, K. B., Reeves, E. P., Sutcliffe, C. N., Ritter, D. J., Seewald, J. S., McIntosh, J. C., Hemond, H. F., Kubo, M. D., Cardace, D., Hoehler, T. M., and Ono, S.: Nonequilibrium clumped isotope signals in microbial methane, Science, 348, 428–431, 2015.

Watts, J. D., Gauss, J., and Bartlett, R. J.: Coupled-cluster methods with noniterative triple excitations for restricted open-shell Hartree–Fock and other general single determinant reference functions. Energies and analytical gradients, J. Chem. Phys., 98, 8718–8733, 1993.

Wigner, E.: On the quantum correction for thermodynamic equilibrium, Phys. Rev., 40, 749–759, 1932.

Woon, D. E. and Dunning Jr., T. H.: Gaussian basis sets for use in correlated molecular calculations. III. The atoms aluminum through argon, J. Chem. Phys., 98, 1358–1371, 1993.

York, D., Evensen, N. M., Martínez, M. L., and De Basable Delgado, J.: Unified equations for the slope, intercept, and standard errors of best straight line, Am. J. Phys., 72, 367–375, 2004.